Threshold friction velocity influenced by soil particle size within the Columbia Plateau, northwestern United States Postprint

Authors: MENG Ruibing

Date: 2024-08-14T00:00:00+00:00

Abstract

Wind erosion is a geomorphic process in arid and semi-arid areas and has substantial implications for regional climate and desertification. In the Columbia Plateau of northwestern United States, the emissions from fine particles of loessial soils often contribute to the exceedance of inhalable particulate matter (PM) with an

Full Text

Preamble

Journal of Arid Land (2024) 16(8): 1147-1162
https://doi.org/10.1007/s40333-024-0081-4
Science Press & Springer-Verlag

Threshold friction velocity influenced by soil particle size within the Columbia Plateau, northwestern United States

MENG Ruibing[1,2,3], MENG Zhongju[1,2,3*], Brenton SHARRATT[4], ZHANG Jianguo[5], CAI Jiale[1,2,3], CHEN Xiaoyan[6]

[1] College of Desert Control Science and Engineering, Inner Mongolia Agricultural University, Hohhot 010018, China
[2] Key Laboratory of Aeolian Physics and Desertification Control Engineering from Inner Mongolia Autonomous Region, Inner Mongolia Agricultural University, Hohhot 010018, China
[3] Key Laboratory of Desert Ecosystem Conservation and Restoration, State Forestry and Grassland Administration of China, Inner Mongolia Agricultural University, Hohhot 010018, China
[4] Inner Mongolia Autonomous Region Academy of Social Sciences, Hohhot 010010, China

Abstract

Wind erosion is a geomorphic process in arid and semi-arid areas with substantial implications for regional climate and desertification. In the Columbia Plateau of northwestern United States, emissions from fine particles of loessial soils often contribute to exceedances of inhalable particulate matter (PM) with an aerodynamic diameter of 10 m or less (PM_{10}) according to air quality standards. However, little is known about the threshold friction velocity (TFV) for particles of different sizes that comprise these soils. In this study, soil samples of two representative soil types (Warden sandy loam and Ritzville silt loam) collected from the Columbia Plateau were sieved into seven particle size fractions, and an experiment was conducted to determine the relationship between TFV and particle size fraction. The results revealed that soil particle size significantly affected the initiation of soil movement and TFV; TFV ranged from 0.304-0.844 m/s and 0.249-0.739 m/s for different particle size fractions of Ritzville silt loam and Warden sandy loam, respectively. PM_{10} and total suspended particulate (TSP) emissions from a bed of 63-90 m soil particles were markedly higher for Warden sandy loam than for Ritzville silt loam. Together with the lower TFV of Warden sandy loam, dust emissions from fine particles (<100 m in diameter) of Warden sandy loam may thus be a main contributor to dust in the region’ s atmosphere, since PM_{10} emissions from soil erosion surfaces and their ensuing suspension within the atmosphere constitute an essential process of soil erosion in the Columbia Plateau. Developing and implementing strategic land management practices on sandy loam soils is therefore necessary to control dust emissions in the Columbia Plateau.

Keywords: particle size; threshold friction velocity; inhalable particulate matter; total suspended particles; Warden sandy loam; Ritzville silt loam; Columbia Plateau

Citation: MENG Ruibing, MENG Zhongju, Brenton SHARRATT, ZHANG Jianguo, CAI Jiale, CHEN Xiaoyan. 2024. Threshold friction velocity influenced by soil particle size within the Columbia Plateau, northwestern United States. *Journal of Arid Land*, 16(8): 1147-1162. https://doi.org/10.1007/s40333-024-0081-4

*Corresponding author: MENG Zhongju (E-mail: mengzj@imau.edu.cn)

Received 2024-03-08; revised 2024-06-14; accepted 2024-06-18

Introduction

The Columbia Plateau is a vast basalt floodplain with complex topography spanning Washington, Oregon, and Idaho in northwestern United States. Loess and sand deposits containing high levels of inhalable particulate matter dominate the soils of the Columbia Plateau (Goudie and Middleton, 2006; McDonald et al., 2012; Kawai et al., 2021). The arid areas of the Columbia Plateau have serious wind erosion problems, mainly caused by poor soil aggregation and frequent high-wind events (Pi et al., 2018). Agricultural soils in most arid areas are managed through a crop rotation system involving winter wheat and summer fallow periods. The lack of vegetation cover during the summer fallow phase of this rotation greatly increases soil susceptibility to wind erosion (Colazo and Buschiazzo, 2015; Chang et al., 2023).

Wind erosion removes fertile topsoil and emits fine particles that degrade air and soil quality, causing varying degrees of harm and even catastrophic damage to the environment (Colazo and Buschiazzo, 2010). Based on their intrinsic physicochemical properties, atmospheric dust particles degrade visibility and air quality, which can lead to road closures and respiratory illnesses (Xing and Guo, 2008; Tominaga and Okuyama, 2022). Wind erosion has caused exceedances of inhalable PM with an aerodynamic diameter of 10 m or less (PM_{10}) according to national air quality standards in the Columbia Plateau (Hwang et al., 2017; Kok et al., 2018).

PM_{10} and fine PM persist in the atmosphere for prolonged periods, significantly impacting human health and atmospheric visibility (Field et al., 2010; Feng et al., 2011; Shao and Klose, 2016). Accordingly, rigorous methods are needed to assess and simulate the dynamics of fine PM emissions from soil during high-wind events (Tominaga, 2022). With the global focus on climate change, desertification, and land degradation, current research continues to emphasize modeling wind erosion and dust emission processes in agricultural and prairie environments (Borrelli et al., 2021). Feng and Sharratt (2007) adopted the Wind Erosion Prediction System (WEPS) to agricultural lands within the Columbia Plateau with varying degrees of success, discovering that WEPS accurately simulated wind erosion only during three of six high-wind events that resulted in significant soil loss and appeared to overestimate soil loss. Pi et al. (2022) subsequently improved prediction accuracy by replacing the calculation component for threshold friction velocity (TFV) in the WEPS model and quantitatively assessed spatio-temporal patterns of wind erosion and PM_{10} emissions using Geographic Information System (GIS) in arid areas of northwestern United States (Pi et al., 2020a). They expressed the need to further understand soil erodibility dynamics in simulating wind erosion.

Wind erosion is sensitive to changes in soil erodibility (Tanner et al., 2023). Indeed, wind erosion and PM_{10} emissions are greatly influenced by soil surface aggregate or particle size (Wang et al., 2019; Pi et al., 2023). TFV is a highly critical parameter in the wind erosion process that determines the frequency and intensity of wind erosion events (Zhang et al., 2021b). As wind speed increases and approaches TFV, changes in turbulence and drag forces result in movement of particles on the soil surface. TFV is the minimum wind speed necessary to initiate sand particle movement along the soil surface (Kouchami-Sardoo et al., 2019). For stationary particles, motion is achieved when drag and uplift forces overcome gravity acting upon the particles and cohesive forces acting between particles on the soil surface. The primary equipment for sand particle motion threshold analysis is the wind tunnel, which determines the frictional velocity of sand particle groups with different average diameters at the threshold using empirical curves of dimensionless Reynolds number functions (Bagnold, 1941). However, Miller and Komar (1977) discovered that the sharp upturn in TFV for fine particles occurs because of particle cohesion rather than Reynolds number effects. In addition, Shao (2001) found that variation of dust emission efficiency with wind speed was related to soil conditions. Therefore, researchers have conducted a series of field experiments and wind tunnel studies to investigate TFV of different textured soils under various soil conditions (wetness, standing crop residue, and tillage systems, etc.) (Feng and Sharratt, 2009; Sharratt et al., 2013; Wang et al., 2019). Although these studies have provided valuable insights into soil erosion, a deeper understanding of soil erodibility across varying particle sizes is crucial for enhancing comprehension and modeling of wind erosion. The size and stability of aggregates determine the degree of soil vulnerability to wind and water erosion. Therefore, determining fluctuations in TFV across different soil particle sizes is imperative, as it will aid in implementing more effective soil conservation strategies to minimize hazards posed by wind erosion.

TFV differs significantly among soils due to differences in cohesion and roughness. In general, TFV decreases and then increases with soil particle size, with soil particles in the 120-140 m size fraction having the lowest TFV (Yue et al., 2012). The magnitude of TFV largely determines surface soil erodibility. Marticorena et al. (1997) established a model to explain TFV for particles 60-120 m in diameter and found that the most influential parameter affecting TFV was aerodynamic roughness length. Etyemezian et al. (2019) calculated TFV based on a surface roughness correction factor to avoid underestimating TFV of rough surfaces. However, aerodynamic roughness length tends to vary during the wind erosion process and is mainly dependent on aggregate or particle size distribution.

Tillage during the summer fallow phase of the winter wheat-summer fallow rotation in the Columbia Plateau can degrade aggregates and soil structure. Thus, the impact of tillage on changes in soil properties affecting wind erosion is the central focus of soil erodibility research in the region (Sharratt and Feng, 2009). Sharratt and Vaddella (2014) determined that TFV for sandy loam and silt loam soils in the Columbia Plateau varied from 0.140 to 0.240 m/s, suggesting that TFV varied as a result of differences in soil texture, environmental conditions, and anthropogenic disturbance. This study expands upon previous research in the Columbia Plateau by assessing the link between TFV and particle size of soils commonly found in the region. The focus was placed on refinement analysis of soil particles (<100 μm), with the aim to further reveal the effect of fine particle size on TFV and provide a scientific basis for developing more targeted soil conservation measures in the Columbia Plateau.

2.1 Soil Preparation and Experimental Design

The experiment was conducted in the summer of 2023 on farmlands near Washington in the Columbia Plateau, where a semi-arid climate dominates and soils are composed of loess and sand deposits. In this study, we collected soil samples of two contrasting soil types representative of the Columbia Plateau. The sampling plot for Warden sandy loam (Mesic Xeric Haplocambids) was near Paterson, Washington (46°10′N, 119°37′W) with annual precipitation of 200 mm. The sampling plot for Ritzville silt loam (Andic Aridic Haplustoll) was near Ritzville, Washington (47°80′N, 118°28′W) with annual precipitation of 280 mm. Both sampling plots were subject to a winter wheat-summer fallow rotation. During the fallow phase of the rotation, each plot was managed by wheat growers employing different tillage practices to control weeds and preserve soil moisture. Warden sandy loam has a higher sand content (67.52%) and lower clay content (9.21%) than Ritzville silt loam (with sand content of 30.53% and clay content of 11.42%). Dispersed particle size analysis using a Malvern Mastersizer laser diffractometer indicated that Warden sandy loam had a geometric mean diameter of 36 mm while Ritzville silt loam had a mean diameter of 20-29 mm (Sharratt and Vaddella, 2014).

Five sampling points were established using the 'S' soil sampling method in each plot. Soil samples collected from the top 1 cm of soil from multiple sampling points in each plot were processed to obtain the erodible portion. Soil samples were air-dried at 70.00°C and then hand-sieved to collect particle size fractions of <45, 45-63, 63-90, 90-125, 125-150, 150-250, and 250-500 m. This study used a portable wind tunnel (working section: 1.00 m width, 1.20 m height, and 7.30 m length) to produce free-stream wind speeds of 2-20 m/s to evaluate TFV [FIGURE:1]. The test section featured plexiglass windows and removable metal trays. The bottom of the wind tunnel was lined with sandpaper, mimicking the roughness of the soil surface in the trays. The wind tunnel was located inside a non-regulated climate facility, where relative humidity and temperature varied from 37.42% to 45.23% and 2.32°C to 13.11°C, respectively, during the experiment. The wind tunnel conditioned winds to resemble naturally occurring shear flow characteristics in the field. Wind was conditioned by flowing through a perforated plate to control vortex and velocity fluctuations, a honeycomb frame and wire mesh to reduce turbulence, and then non-uniform mesh components to create shear flow (Pietersma et al., 1996). The wind tunnel floor was built from wood coated with fine sand to simulate boundary layer features of natural bare soil surfaces. A 20 mm deep soil tray was recessed into the wooden floor 5.00 m downwind from the grill component so that the tray top remained level with the wooden floor.

The soil trays and wooden floor were constructed with precision to minimize any gap between them. Soil composed of a specific size fraction of particles was placed in the 1.00 m × 0.20 m × 0.02 m metal soil tray, and the top of the tray was then smoothed with a metal screed.

[FIGURE:1]

2.2 Wind Tunnel Assessment

Wind speed was measured utilizing a pressure transducer connected to a pitot tube mounted at six different heights (5, 10, 20, 30, 50, and 100 mm) above the soil surface at the leeward edge of the soil tray. Wind speed was corrected for atmospheric pressure and temperature that varied during the experiment. Sensor technology was used instead of visual observation to measure particle emissions from the soil tray because PM emitted from the soil surface was too small to be visible to the naked eye. Simultaneous observations of PM_{10} and total suspended particulate (TSP) concentrations (mg/m^3) were made at the leeward edge of the soil tray using the DUSTTRAK Aerosol Monitor (Model 8520, TSI Incorporated, Shoreview, USA) and E-sampler (Met One Instruments, Inc., Grants Pass, USA), respectively. Particulate sensors were mounted at the same height above the soil surface as wind speed sensors, similar to previous studies (Copeland et al., 2009). The emission of soil particles from the tray as a function of wind speed was also monitored using a Sensit (Model H11-LIN, Sensit Company, Portland, USA). The Sensit was installed at a height of 50 mm above the soil surface. The entrance of the tunnel construction section was also equipped with particulate monitors for measuring background concentrations of PM_{10} and TSP. Ambient dust concentrations in the wind tunnel facility were consistently low throughout the experiment. All sensors were programmed to record experimental parameters every second.

2.3 TFV Determination

TFV for each soil particle size fraction was determined by detecting the rise in PM_{10} and TSP concentrations downwind of the soil tray over background concentrations within a period of several seconds. In the wind tunnel, TSP concentration remained essentially constant as wind speed increased. When wind speed reached TFV, PM_{10} and TSP concentrations exceeded background concentrations at several heights. TFV was measured by systematically raising the wind speed every 15 s until an increase in PM_{10} or TSP concentration above background was observed for multiple seconds. This procedure ensures that a critical shear stress is reached, which allows particles or agglomerates to be released from the soil surface. This method of TFV determination (Sharratt et al., 2013) differs from visual inspection, which is probably more appropriate for detecting apparent movement of larger particles on the soil surface (Gillette and Passi, 1988). In some instances, saltation activity can facilitate assessing TFV, though no saltation activity was observed using the Sensit in this study. Once PM_{10} or TSP concentration rose above background concentrations during a 15 s period, the experiment continued for 15 s to validate observations. The experiment was replicated four times for each soil type and particle size fraction. The water potential of the soil surface in the tray was measured immediately before the soil was exposed in the wind tunnel, and wind speed was reduced after each experiment. Although the duration of each measurement was short (averaging about 300 s), this method obtained the range of water potential for each soil type and particle size fraction during the experiment. Soil water potential was measured using either a dew point meter (WP4T, Decagon Devices, Pullman, Washington, USA) or filter paper technique (ASTM D5298-10, 2010). Fawcett and Collis-George (1967) verified that the filter paper technique is reliable and accurate. The soil in the tray was discarded after each replication. Wind speed profile parameters were calculated using wind speed data collected at the six heights. Wind speed profile was fitted according to Prandtl-von Karman' s logarithmic law (Roney and White, 2006), and friction velocity and aerodynamic roughness length were experimentally determined from the wind speed profile based on the following equation:

$$)\ln(/$$

where u_z is wind speed (m/s) at height z (m); u_* is the friction velocity (or shear velocity) (m/s); k is von Karman' s constant ($k = 0.4$); and z_0 is the aerodynamic roughness length (m).

Aerodynamic roughness lengths for different particle sizes were determined by plotting the natural logarithm of height against wind speed (Dong et al., 2002). The optimal fit was determined through regression analysis using the least squares method and expressed mathematically as:

where a and b are the regression coefficients, which are used to define the aerodynamic roughness length according to:

Combining Equations 1-3, friction velocity can be calculated as:

PM_{10} and TSP concentrations above background concentrations were typically found within 180-300 s of generating winds inside the wind tunnel. This procedure attempted to eliminate errors introduced by contamination or singular or 1 s transient increases or peaks in PM_{10} or TSP concentration due to emission of perched particles on the soil surface. Approximately 60 s was required to install the soil tray in the wind tunnel floor and ready all instrumentation before generating winds to determine TFV. TFV (m/s) was determined from the friction velocity within 15 s after PM_{10} or TSP concentration exceeded the above-background value.

3.1 Variations in PM_{10} and TSP Concentrations with Particle Size Fraction for the Two Representative Soils

Figures 2 and 3 show variations in PM_{10} and TSP concentrations with particle size fraction for Warden sandy loam and Ritzville silt loam. During the experiment, PM_{10} and TSP concentrations changed dramatically with wind speed as TFV was attained. Specifically, when wind speed exceeded TFV, Warden sandy loam showed the highest TSP and PM_{10} concentrations for particle size fractions of 63-90, 90-125, and 125-150 m. The highest TSP and PM$_{10}$ concentrations for Ritzville silt loam were observed in particle size fractions of 125-150 and 150-250 m, respectively. This suggested that particles in the 63-150 m size fraction for Warden sandy loam and in the 125-250 m size fraction for Ritzville silt loam were most vulnerable to generating PM$_{10}$ emissions. Notably, PM$_{10}$ and TSP emissions from Warden sandy loam were significantly higher than those from Ritzville silt loam when particle size was below 150 m. This suggested that PM$_{10}$ attached to Warden sandy loam tends to be released more rapidly than that attached to Ritzville silt loam under high shear stress or as a result of saltation bombardment. This difference may stem from varying soil textures, as Warden sandy loam has higher sand particle content (67.52%) than Ritzville silt loam (with sand content of 30.53%). Soils rich in sand content often lack aggregates, making it easy for fine particles to detach from sand grains, thus becoming a significant source of PM$_{10}$ emissions. Indeed, sandy soils with weak cohesive characteristics are more fragile and likely susceptible to bombardment compared to silty soils with stronger bonding characteristics. Additionally, soils with higher sand content show excellent water permeability and aeration. The absolute values of the rate of change in water potential of Warden sandy loam were significantly higher than those of Ritzville silt loam . This indicates that sandy loam has stronger hydrophobicity and weaker water film binding force. Therefore, we assumed that both low particle forces and low aggregation can increase TSP emissions significantly.

Soils of different textures exhibited significant differences in PM$_{10}$ and TSP emissions across varying particle size fractions. PM$_{10}$ and TSP emissions from Warden sandy loam were significantly higher than those from Ritzville silt loam in most particle size fractions. However, in the 150-250 m size fraction, PM$_{10}$ and TSP emissions from Ritzville silt loam were higher than those from Warden sandy loam. Notably, unlike Warden sandy loam, which has higher sand content, aggregate fragmentation became the dominant process in the clay-rich soil of Ritzville silt loam.

Interestingly, the highest PM$_{10}$ and TSP emissions were found in the 125-150 m size fraction for both soils. This may indicate that, compared to soils with smaller or larger particle sizes, soils with medium texture experience collective processes where detachment of dust attached to the soil surface, fragmentation of aggregates, and bombardment of saltating particles may together lead to continuous emissions of PM$_{10}$ and TSP. Therefore, we hypothesized that soil particles in the 125-150 m size fraction were the predominant source of high PM$_{10}$ concentrations in the Columbia Plateau

. This provides a new perspective for further research and controlling environmental pollution in the region.

Although the Sensit was used to detect potential saltation activity, there was a lack of saltation activity in our wind tunnel experiment. This is probably due to the limited size of the soil tray and sensitivity constraints of the sensors, rather than an actual lack of saltation activity. Suspension at low wind speeds is

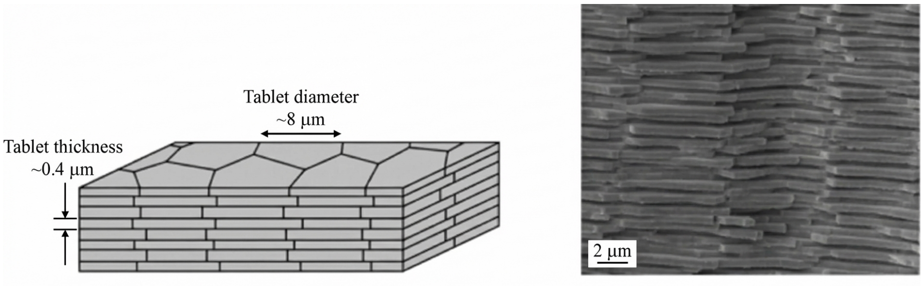

(a) Schematic diagram of layered arrangement (b) SEM microstructure of pearl fracture surface

Figure 1: Figure 4

generally considered a minor component of total dust flux because surface wind speeds are probably insufficient to overcome interaction forces between fine particles, including capillary forces. In the case of PM_{10} emissions from finer soils, we postulated that the suspension mechanism holds greater significance. Finer soil particles are more easily lifted by wind and suspended in the air, ultimately contributing to PM_{10} emissions. Conversely, in coarser soils, PM_{10} generation is predominantly driven by processes such as bombardment and abrasion, marking a distinct contrast in PM_{10} generation mechanisms. However, we cannot confirm that direct suspension will cause an increase in PM_{10} and TSP emissions. Although particle size and number can affect saltation activity, Van Pelt et al. (2009) found that the Sensit was not sensitive to particles smaller than 100 m in diameter except at very high wind speeds. Moreover, Sharratt (2011) suggested that the Sensit lacked sensitivity for saltating particles smaller than 100 m in diameter that are commonly found in windblown dust in the Columbia Plateau. Thus, saltation may have occurred but was not detected with our instrumentation.

3.2 TFV of the Two Representative Soil Types in Different Particle Size Fractions

Figure 5 illustrates wind speed profiles of the two representative soil types across varying particle size fractions. The good fit ($R^2 > 0.918$) of the wind speed profile data provided confidence in estimating TFV and aerodynamic roughness length. TFV of Ritzville silt loam and Warden sandy loam ranged from 0.304 to 0.844 m/s and 0.249 to 0.739 m/s, respectively, across all particle size fractions. TFV is related to particle size, particle shape, and microstructure of the soil surface (Wang et al., 2008). The highest TFV for Ritzville silt loam occurred in the <45 m size fraction, while the highest TFV for Warden sandy loam occurred in the 45-63 m size fraction. The increasing trend in TFV with soil particle size fraction was significantly different between the two soil types.

TFV of the two soil types in different particle size fractions is shown in Figure 6. For the 45-63 m size fraction, TFV differed between the two soil types,

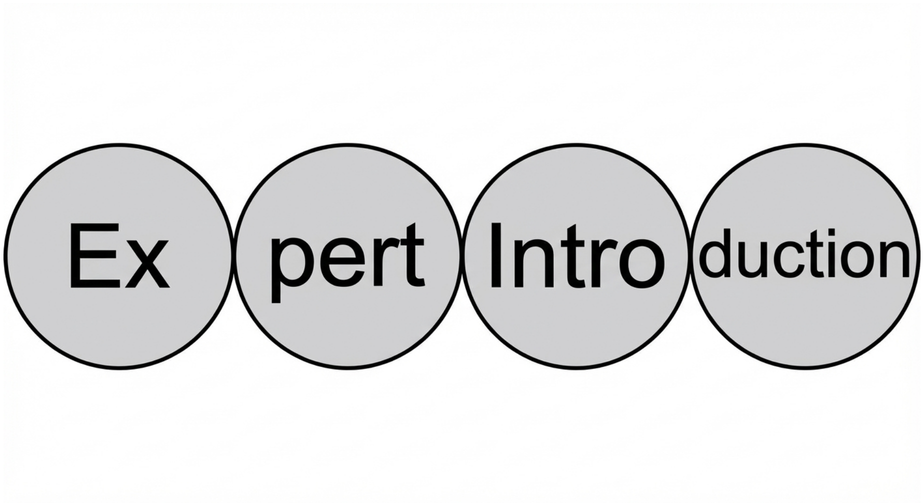

Figure 2: Figure 2

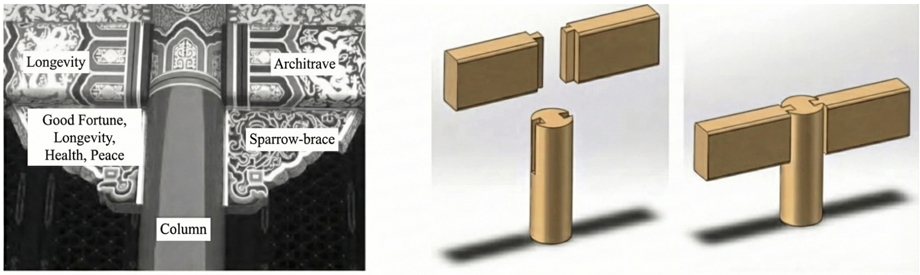

(a) Mortise and tenon connection between the column and architrave of the Hall of Supreme Harmony in the Forbidden City

(b) Schematic diagram of the dovetail mortise and tenon connection

Figure 3: Figure 3

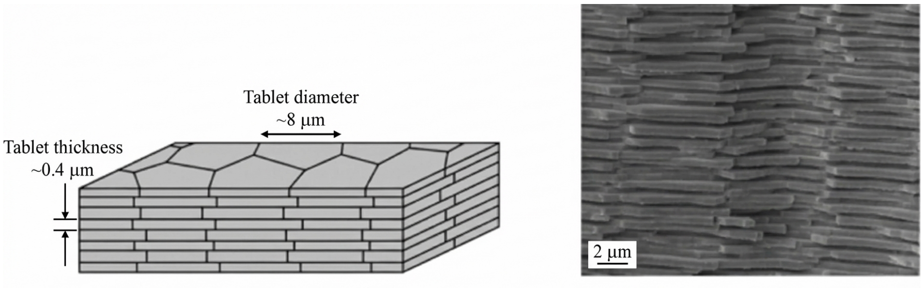

(a) Schematic diagram of layered arrangement

(b) SEM microstructure of pearl fracture surface

Figure 4: Figure 4

being significantly higher for Warden sandy loam (0.749 m/s) than for Ritzville silt loam (0.526 m/s). This difference in TFV may be related to differences in cohesive forces between soil aggregates (Greeley and Iversen, 1985; Colazo and Buschiazzo, 2010). In the 125-150 m size fraction, Warden sandy loam had a lower TFV than Ritzville silt loam. In fact, the lowest TFV for both soil types occurred in the 250-500 m size fraction. TFV in the 250-500 m size fraction was 64.01% and 66.27% lower than that in the <45 m size fraction for Ritzville silt loam and Warden sandy loam, respectively.

In our study, exponential functions adequately described the relationship between TFV and particle size fraction ($R^2 \geq 0.867$), which can be used to estimate the response of TFV to particle size for the two soil types [FIGURE:6]. The standard errors of the fitted equation for both soil types ranged between 0.03 and 0.09 m/s. Estimating TFV under known smooth, dry, fine-grain, loose, and bare soil surface conditions can be very effective. Accordingly, as soil particle size increased from 45 to 500 m, TFV decreased for both soil types. Significant differences in TFV between the two soil types were observed in the same particle size fraction after saltation, because particle emission may also occur before the soil tray is placed in the wind tunnel, which corresponds to the static threshold observed during particle shaking. After the saltation process, Ritzville silt loam had the largest decrease in TFV when the particle size fraction varied from <45 to 45-63 m. In contrast, Warden sandy loam had the largest decrease in TFV as the particle size fraction varied from 45-63 to 63-90 m. These observations indicated that the largest differences in TFV can be found for particles smaller than 100 m in size for the two soil types.

[FIGURE:5]
[FIGURE:6]

3.3 Relationship Between Aerodynamic Roughness Length and TFV

Aerodynamic roughness length reflects the weakening effect of the soil surface on wind speed as well as wind and sand activity (Dong et al., 2002). It is related to the size of particles or aggregates on the soil surface. As aggregates or particles on the soil surface become larger, aerodynamic roughness length increases. Figure 7 shows that aerodynamic roughness length increased with soil particle size for the two representative soil types. The aerodynamic roughness length of Ritzville silt loam and Warden sandy loam increased by 0.043 and 0.049 mm, respectively, as particle size increased from the smallest size fraction (<45 m) to the largest size fraction (250-500 m). These results indicated that as particle size increases, the destructive force of the soil surface against airflow increases, resulting in a rougher surface that can better trap and immobilize soil particles, thus reducing wind erosion.

Etyemezian (2019) indicated that aerodynamic roughness length can affect TFV. As shown in Figure 8, even within a narrow range of aerodynamic roughness length, TFV exhibited noticeable variations. Specifically, the intercept of the relationship between TFV and aerodynamic roughness length was -1.151 m/s for Ritzville silt loam and -0.742 m/s for Warden sandy loam, indicating that TFV is greater for Warden sandy loam than for Ritzville silt loam with very little aerodynamic roughness length. Additionally, Figure 8 reveals a negative correlation between aerodynamic roughness length and TFV, indicating that a decrease in aerodynamic roughness length leads to an increase in TFV. This result may seem counterintuitive, as the TFV derived in this study focused on inhalable PM emissions from isolated soil particles of different size fractions rather than the traditional soil erosion threshold. From a physical perspective, friction velocity is determined by the momentum transferred by the surface with a certain geometric roughness after absorbing the shear stress of the boundary layer flow. Therefore, changes in wind momentum absorbed by the erodible components of the soil surface will cause a change in friction velocity. The aerodynamic roughness length generated by surface geometric roughness is the main factor affecting friction velocity. This study revealed that finer soil fractions correspond to smaller aerodynamic roughness length.

[FIGURE:8]

3.4 Further Analysis of Factors Affecting TFV

In arid and semi-arid areas, the impact of wind erosion on soil is a crucial factor shaping the landscape and biological potential of the surface (Shao, 2000; Chandler et al., 2004; Ebrahimi-Khusfi and Soleimani Sardoo, 2021). The size and stability of soil aggregates directly determine the sensitivity of soil to wind and water erosion (Kheirabadi et al., 2018; Yang et al., 2022; Zhu et al., 2022). This study found that TFV of isolated particles in different size fractions was higher than previously reported results in the Columbia Plateau. For instance, Sharratt and Vaddella (2012) found that TFV of Warden sandy loam was 0.139 m/s and TFV of Ritzville silt loam was 0.180-0.239 m/s. This phenomenon may be attributed to the special properties of the soil particles in this study. The soil particles obtained through fine screening are smaller and have a uniform particle size distribution, which significantly reduces gaps between particles and results in a compact structure. Under the same wind speed conditions, this compact structure makes it more difficult for soil particles to be blown away by wind, leading to higher TFV. Furthermore, experiments by Bagnold (1941) provided valuable insights: even if wind speed is sufficient to move fine stones with a diameter of 4600 m, it is still difficult to blow finer cement sand in stable airflow. The relationship between TFV and particle size is complex and not directly proportional. Larger particles generally require higher wind speeds to be blown away due to increased mass and inertia, but other factors also play a role. For example, particle shape, soil moisture, and the presence of other particles can all affect TFV (Tanner et al., 2018; Pi et al., 2020b). In our study, the particle size on the soil surface is relatively uniform, and a very smooth surface is formed after ironing treatment. This treatment results in a more uniform

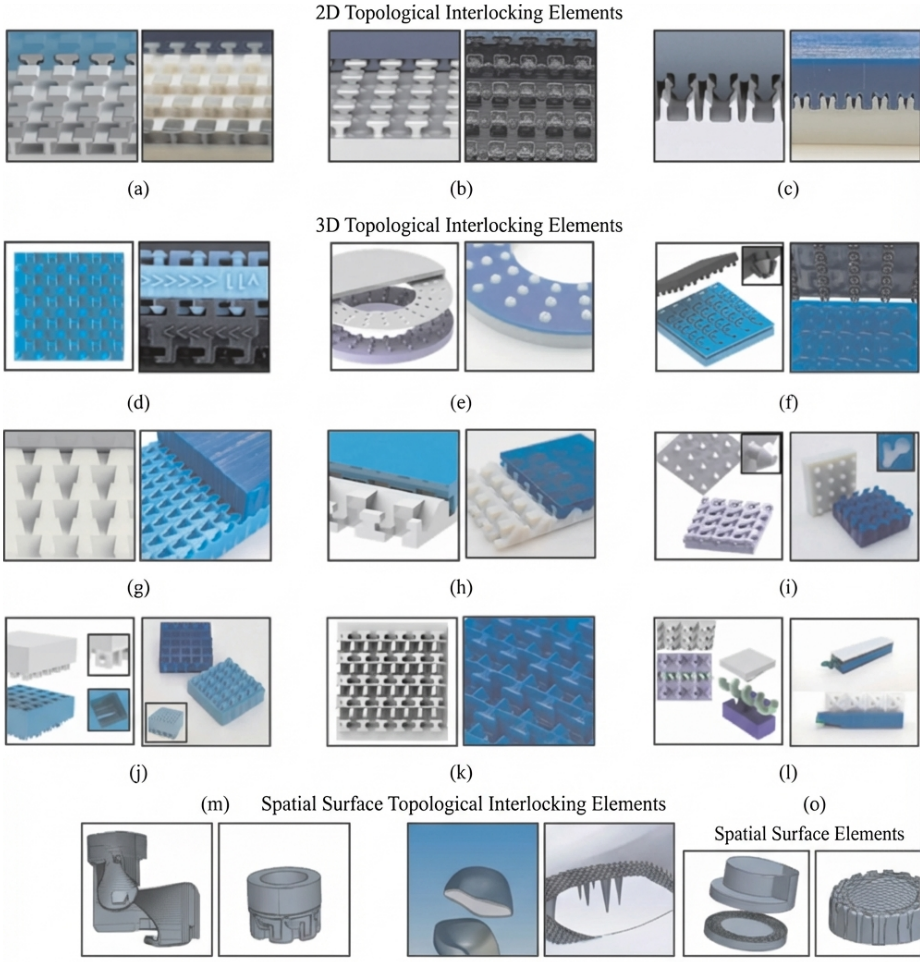

Fig. 2.2 Schematic diagram of typical topological interlocking element designs

Figure 5: Figure 7

distribution of resistance across the entire soil bed, which has a profound impact on TFV measurement results. Additionally, the lack of particles susceptible to direct wind influence on the soil surface may also contribute to the higher TFV observed in this study.

Meanwhile, soil wind erosion is a complex phenomenon since it involves numerous interacting factors (Kjelgaard et al., 2004; Sundram et al., 2004; Zamani and Mathmoodabadi, 2013). Shao (2008) indicated that particle size distribution, soil wetness, soil surface roughness, aboveground biomass, and crust cover influence TFV. The interaction of these factors determines the sensitivity of soil to wind erosion. Especially on dry, loose sand surfaces, TFV is mainly influenced by the particle size of sand grains. If particles are small enough, they will adhere well upon contact even when completely dry, particularly in a vacuum. TFV of Ritzville silt loam and Warden sandy loam ranged from 0.304 to 0.844 m/s and 0.249 to 0.739 m/s, respectively, across particle size fractions in this study. We speculate that the difference in TFV between different particle size fractions of the two soil types may be partially attributed to variations in soil particle cohesion. Especially in fine-grained soils, cohesion is deeply influenced by intermolecular forces, including van der Waals forces, electrostatic forces, and capillary forces. Due to the large specific surface area of fine-grained soils, these intermolecular forces become more significant. In addition, different soil particle sizes have variable degrees of water repellency or hydrophobicity, with finer-grained materials requiring more suitable soil moisture (Sharratt, 2007; Ishizuka et al., 2008; Ravi et al., 2016). Interparticle capillary force is the primary factor resulting in increased TFV when soil moisture increases, and fine-grained soils retain more water than large-particle soil aggregates. We observed an average decrease of 8.99% in water potential for the two soil types in the <45 m size fraction, while an average decrease of 33.32% was observed in the 250–500 m size fraction. Interparticle cohesion plays a crucial role in wind erosion of fine-grained materials (Colazo and Buschiazzo, 2010). As a result, moisture bonding and soil cohesion between soil particles in the <45 m size fraction is much greater than that in the 250–500 m size fraction, resulting in higher TFV.

Wind erosion generates dust, which serves as a significant source of atmospheric aerosols (Zhang et al., 2022; Gao et al., 2023). Agricultural practices that denude or disturb soil in arid areas can therefore lead to environmental degradation. Potential dust emission is a complex yet crucial topic. According to previous studies, PM_{10} emissions increase with silt and clay content and decrease with sand content, and differences in PM_{10} emissions may be related to variations in soil organic matter content, aggregate size distribution, and aggregate stability (Funk et al., 2008; Avecilla et al., 2016; Zhang et al., 2021a). This paper examined two representative soil types, unveiling a profound correlation between distinct soil particle size fractions and PM_{10} and TSP emissions. Our findings revealed that both PM_{10} and TSP emissions attain their apex for the two soil types when soil particle size falls between 125 and 150 m. This suggested that a substantial amount of fine PM becomes suspended during the wind erosion process. It is widely accepted that the interaction between saltation components and soil surface largely depends on their composition, aggregation state, or strength during wind erosion and dust emission processes. Our results align with this consensus, emphasizing the crucial role of high PM_{10} concentration and low aggregation in determining dust emission rates, especially highlighting the importance of soil particles in the 125-150 m size fraction in dust generation. Once these complex particles or aggregates are set in motion by wind force, they can exhibit distinct behaviors in terms of PM_{10} emissions.

4 Conclusions

The Columbia Plateau is severely impacted by wind erosion. Sediment generated by wind erosion of farmlands remains suspended in the air and is the major cause of poor air quality and visibility during periods of high winds. Therefore, ascertaining when sediment is emitted from the soil surface into the atmosphere is paramount to controlling wind erosion, but further research is needed to investigate variation in TFV of diverse soils in the Columbia Plateau. The results showed that TFV of Ritzville silt loam and Warden sandy loam in different particle size fractions ranged from 0.304 to 0.844 m/s and 0.249 to 0.739 m/s, respectively. We also found that TFV for the smallest size fraction (<45 m) was significantly higher than that for the largest size fraction (250-500 m) for both soil types. Therefore, soil particle size can dramatically affect soil wind erosion due to differences in TFV among particle sizes. Soil particles in the 125-150 m size fraction are the primary source of high PM_{10} concentrations in the Columbia Plateau, and suspended sediments appear to constitute the majority of wind-blown sediments in this region, thereby elevating the risk of air quality deterioration. Therefore, it is imperative to advance and enforce strategic land management practices aimed at mitigating dust emissions in the Columbia Plateau to promote sustainable crop production in this region.

Conflict of Interest

The authors declare that they have no known competing financial interests or personal relationships that could have appeared to influence the work reported in this paper.

Acknowledgements

This research was supported by the Basic Research Funds for Colleges and Universities directly under the Inner Mongolia Autonomous Region: Desert Ecosystem Protection and Restoration Innovation Team (BR 22-13-03).

Author Contributions

Conceptualization: MENG Ruibing, MENG Zhongju, Brenton SHARRATT
Data curation: MENG Ruibing, ZHANG Jianguo

Formal analysis: CAI Jiale
Funding acquisition: MENG Zhongju
Investigation: MENG Ruibing, MENG Zhongju, ZHANG Jianguo
Methodology: Brenton SHARRATT, ZHANG Jianguo
Supervision: MENG Zhongju, Brenton SHARRATT
Validation: CAI Jiale, CHEN Xiaoyan
Visualization: MENG Ruibing, CAI Jiale, CHEN Xiaoyan
Writing -original draft: MENG Ruibing
Writing -review & editing: MENG Zhongju, Brenton SHARRATT

All authors approved the manuscript.

References

ASTM D5298-10. 2010. Standard test method for measurement of soil potential (suction) using filter paper. ASTM International, West Conshohocken, PA, USA.

Avecilla F, Panebianco J E, Buschiazzo D E. 2016. A wind-tunnel study on saltation and PM_{10} emission from agricultural soils. *Aeolian Research*, 22: 73-83.

Bagnold R A. 1941. *The Physics of Blown Sand and Desert Dunes*. London: Methuen, 91-96.

Borrelli P, Alewell C, Alvarez P, et al. 2021. Soil erosion modelling: A global review and statistical analysis. *Science of the Total Environment*, 780: 146494, doi: 10.1016/j.scitotenv.2021.146494.

Chandler D G, Blaesing-Thompson S, Busacca A. 2004. Geospatial assessment of agricultural lands critical to air quality on the Columbia Plateau, Washington State. *Journal of Soil and Water Conservation*, 59(4): 184-189.

Chang T T, Feng G, Paul V, et al. 2023. Soil health assessment for different tillage and cropping systems to determine sustainable management practices in a humid region. *Soil and Tillage Research*, 233: 105796, doi: 10.1016/j.still.2023.105796.

Colazo J C, Buschiazzo D E. 2010. Soil dry aggregate stability and wind erodible fraction in a semiarid environment of Argentina. *Geoderma*, 159(1-2): 228-236.

Colazo J C, Buschiazzo D E. 2015. The impact of agriculture on soil texture due to wind erosion. *Land Degradation and Development*, 26(1): 62-70.

Copeland N S, Sharratt B S, Wu J Q, et al. 2009. A wood-strand material for wind erosion control: Effects on total sediment loss, PM_{10} vertical flux, and PM_{10} loss. *Journal of Environmental Quality*, 38(1): 139-148.

Dong Z B, Liu X P, Wang X M. 2002. Aerodynamic roughness of gravel surfaces. *Geomorphology*, 43(1-2): 17-31.

Ebrahimi-Khusfi Z, Soleimani Sardoo M. 2021. Recent changes in physical properties of the land surface and their effects on dust events in different climatic regions of Iran. *Arabian Journal of Geosciences*, 14: 287, doi: 10.1007/s12517-021-06664-9.

Etyemezian V, Gillies J A, Mastin L G. 2019. Laboratory experiments of volcanic ash resuspension by wind. *Journal of Geophysical Research: Atmospheres*, 124(16): 9534–9560.

Fawcett R G, Collis-George N. 1967. A filter-paper method for determining the moisture characteristics of soil. *Australian Journal of Experimental Agriculture*, 7: 162–167.

Feng G L, Sharratt B S. 2007. Validation of WEPS for soil and PM_{10} loss from agricultural fields within the Columbia Plateau of the United States. *Earth Surface Processes and Landforms*, 32(5): 743–753.

Feng G L, Sharratt B S. 2009. Evaluation of the SWEEP model during high winds on the Columbia Plateau. *Earth Surface Processes and Landforms*, 34(11): 1461–1468.

Feng G L, Sharratt B S, Young F. 2011. Soil properties governing soil erosion affected by cropping systems in the U.S. Pacific Northwest. *Soil and Tillage Research*, 111(2): 168–174.

Field J P, Belnap J, Breshears D D. 2010. The ecology of dust. *Frontiers in Ecology and the Environment*, 8(8): 423–430.

Funk R, Reuter H I, Hoffmann C, et al. 2008. Effect of moisture on fine dust emission from tillage operations on agricultural soils. *Earth Surface Processes and Landforms*, 33(12): 1851–1863.

Gao Q Q, Zhu X J, Wang Q H, et al. 2023. Enrichment and transfer of polycyclic aromatic hydrocarbons (PAHs) through dust aerosol generation from soil to the air. *Frontiers of Environmental Science and Engineering*, 17: 10, doi: 10.1007/s11783-023-1610-7.

Gillette D A, Passi R. 1988. Modeling dust emission caused by wind erosion. *Journal of Geophysical Research*, 93(D11): 14233–14242.

Goudie A S, Middleton N J. 2006. *Desert Dust in the Global System.* Heidelberg: Springer, 13–31.

Greeley R, Iversen J D. 1985. *Wind as a Geological Process on Earth, Mars, Venus and Titan.* New York: Cambridge University Press, 33–61.

Hwang S H, Lee J Y, Yi S M, et al. 2017. Associations of particulate matter and its components with emergency room visits for cardiovascular and respiratory diseases. *PLoS ONE*, 12(8): e0183224, doi: 10.1371/journal.pone.0183224.

Ishizuka M, Mikami M, Leys J, et al. 2008. Effects of soil moisture and dried raindroplet crust on saltation and dust emission. *Journal of Geophysical Research: Atmospheres*, 113(D24): D24212, doi: 10.1029/2008JD009955.

Kawai K, Matsui H, Kimura R, et al. 2021. High sensitivity of Asian dust emission, transport, and climate impacts to threshold friction velocity. *Scientific Online Letters on the Atmosphere*, 17: 239-245.

Kheirabadi H, Mahmoodabadi M, Jalali V, et al. 2018. Sediment flux, wind erosion and net erosion influenced by soil bed length, wind velocity and aggregate size distribution. *Geoderma*, 323: 22-30.

Kjelgaard J, Sharratt B, Sundram I, et al. 2004. PM_{10} emission from agricultural soils on the Columbia Plateau: Comparison of dynamic and time-integrated field-scale measurements and entrainment mechanisms. *Agricultural and Forest Meteorology*, 125(3-4): 259-277.

Kok J F, Ward D S, Mahowald N M. 2018. Global and regional importance of the direct dust-climate feedback. *Nature Communications*, 9(1): 241, doi: 10.1038/s41467-017-02620-y.

Kouchami-Sardoo I, Shirani H, Esfandiarpour-Boroujeni I, et al. 2019. Optimal feature selection for prediction of wind erosion threshold friction velocity using a modified evolution algorithm. *Geoderma*, 354: 113873, doi: 10.1016/j.geoderma.2019.113873.

Marticorena B, Bergametti G, Gillette D, et al. 1997. Factors controlling threshold friction velocity in semiarid and arid areas of the United States. *Journal of Geophysical Research: Atmospheres*, 102(D19): 23277-23287.

McDonald E V, Sweeney M R, Busacca A J. 2012. Glacial outburst floods and loess sedimentation documented during Oxygen Isotope Stage 4 on the Columbia Plateau, Washington State. *Quaternary Science Reviews*, 45: 18-30.

Miller M C, Komar P D. 1977. The development of sediment threshold curves for unusual environments (Mars) and for inadequately studied materials (foam sand). *Sedimentology*, 24(5): 709-721.

Pi H W, Sharratt B, Schillinger W F, et al. 2018. Wind erosion potential of a winter wheat-summer fallow rotation after land application of biosolids. *Aeolian Research*, 32: 53-59.

Pi H W, Huggins D R, Abatzoglou J T, et al. 2020a. Modeling soil wind erosion from agro-ecological classes of the Pacific Northwest in response to current climate. *Journal of Geophysical Research: Atmospheres*, 125(2): e2019JD031104, doi: 10.1029/2019JD031104.

Pi H W, Huggins D R, Sharratt B. 2020b. Influence of clay amendment on soil physical properties and threshold friction velocity within a disturbed crust cover in the inland Pacific Northwest. *Soil and Tillage Research*, 202: 104659, doi: 10.1016/j.still.2020.104659.

Pi H W, Webb N P, Lei J, et al. 2022. Soil loss and PM_{10} emissions from agricultural fields in the Junggar Basin over the past six decades. *Journal of Soil and Water Conservation*, 77(2): 113-125.

Pi H W, Webb N P, Huggins D R, et al. 2023. Effects of secondary soil aggregates on threshold friction velocity and wind erosion. *Land Degradation and Development*, 34(1): 16-27.

Pietersma D, Stetler L D, Saxton K E. 1996. Design and aerodynamics of a portable wind tunnel for soil erosion and fugitive dust research. *Transactions of the ASAE*, 39(6): 2075-2083.

Ravi S, Sharratt B S, Li J R, et al. 2016. Particulate matter emissions from biochar-amended soils as a potential tradeoff to the negative emission potential. *Scientific Reports*, 6: 35984, doi: 10.1038/srep35984.

Roney J A, White B R. 2006. Estimating fugitive dust emission rates using an environmental boundary layer wind tunnel. *Atmospheric Environment*, 40(40): 7668-7685.

Shao Y P. 2000. *Physics and Modeling of Wind Erosion*. The Netherlands: Kluwer Academic Publishers, 211-245.

Shao Y P. 2001. A model for mineral dust emission. *Journal of Geophysical Research: Atmospheres*, 106(D17): 20239-20254.

Shao Y P. 2008. *Physics and Modelling of Wind Erosion*. Berlin: Springer, 1-11.

Shao Y P, Klose M. 2016. A note on the stochastic nature of particle cohesive force and implications to threshold friction velocity for aerodynamic dust entrainment. *Aeolian Research*, 22: 123-125.

Sharratt B S. 2007. Instrumentation to quantify soil and PM_{10} flux using a portable wind tunnel. International Symposium on Air Quality and Waste Management for Agriculture, Broomfield, Colorado.

Sharratt B S, Feng G L. 2009. Windblown dust influenced by conventional and undercutter tillage within the Columbia Plateau, USA. *Earth Surface Processes and Landforms*, 34(10): 1323-1332.

Sharratt B S. 2011. Size distribution of windblown sediment emitted from agricultural fields in the Columbia Plateau. *Soil Science Society of America Journal*, 75(3): 1054-1060.

Sharratt B S, Vaddella V K. 2012. Threshold friction velocity of soils within the Columbia Plateau. *Aeolian Research*, 6: 13-20.

Sharratt B S, Vaddella V K, Feng G L. 2013. Threshold friction velocity influenced by wetness of soils within the Columbia Plateau. *Aeolian Research*, 9: 175-182.

Sharratt B S, Vaddella V K. 2014. Threshold friction velocity of crusted windblown soils in the Columbia Plateau. *Aeolian Research*, 15: 227-234.

Sundram I, Claiborn C, Strand T. 2004. Numerical modeling of windblown dust in the Pacific Northwest with improved meteorology and dust emission models. *Journal of Geophysical Research: Atmospheres*, 109(D24): D24208, doi: 10.1029/2004JD004794.

Tanner S, Katra I, Argaman E, et al. 2018. Erodibility of waste (Loess) soils from construction sites under water and wind erosional forces. *Science of the Total Environment*, 616-617: 1524-1532.

Tanner S, Ben-Hur M, Argaman E, et al. 2023. The effects of soil properties and aggregation on sensitivity to erosion by water and wind in two Mediterranean soils. *Catena*, 221: 106787, doi: 10.1016/j.catena.2022.106787.

Tominaga Y, Okuyama T. 2022. Investigating threshold wind velocity for movement of sparsely distributed gravels in a wind tunnel: Effect of surface coarseness. *Aeolian Research*, 54: 100775, doi: 10.1016/j.aeolia.2022.100775.

Van Pelt R S, Peters P, Visser S. 2009. Laboratory wind tunnel testing of three commonly used saltation impact sensors. *Aeolian Research*, 1(1-2): 55-62.

Wang R D, Zhou N, Li Q, et al. 2008. Difference in wind erosion characteristics between loamy and sandy farmlands and the implications for soil dust emission potential. *Land Degradation and Development*, 29(12): 4362-4372.

Wang R D, Li Q, Zhou N, et al. 2019. Effect of wind speed on aggregate size distribution of windblown sediment. *Aeolian Research*, 36: 1-8.

Xing M, Guo L J. 2008. Research on dust emission law in soil wind erosion process. *Scientia Sinica (Physica, Mechanica & Astronomica)*, 38(8): 984-998. (in Chinese)

Yang M N, Tian X, Guo Z L, et al. 2022. Effect of dry soil aggregate size on microplastic distribution and its implications for microplastic emissions induced by wind erosion. *Environmental Science & Technology Letters*, 9(7): 618-624.

Yue G W, Jia H N, Lin H X. 2012. Release mechanism of soil particles in soil wind erosion. *Arid Land Geography*, 35(2): 248-253. (in Chinese)

Zamani S, Mathmoodabadi M. 2013. Effect of particle-size distribution on wind erosion rate and soil erodibility. *Archives of Agronomy and Soil Science*, 59(12): 1743-1753.

Zhang H T, Tian P F, Kang C L, et al. 2022. Regional organic matter and mineral dust are the main components of atmospheric aerosols over the Nam Co station on the central Tibetan Plateau in summer. *Frontiers in Environmental Science*, 10, doi: 10.3389/fenvs.2022.1055673.

Zhang J, Amonette J E, Flury M. 2021a. Effect of biochar and biochar particle size on plant-available water of sand, silt loam, and clay soil. *Soil and Tillage*

Research, 212: 104992, doi: 10.1016/j.still.2021.104992.

Zhang Z C, Dong Z B, Qian G Q, et al. 2021b. Gravel-desert surface properties and their influences on the wind-erosion threshold friction velocity in North-West China. *Boundary-Layer Meteorology*, 179: 117–131.

Zhu X A, Liu W J, Yuan X, et al. 2022. Aggregate stability and size distribution regulate rainsplash erosion: Evidence from a humid tropical soil under different land-use regimes. *Geoderma*, 420: 115880, doi: 10.1016/j.geoderma.2022.115880.

Figures

(a) From left to right: Triangular unit, cosine bone-shaped unit, H+ unit experimental blocks and finite element models

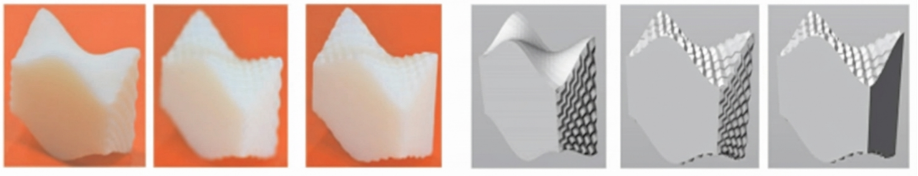

(b) As independent blocks for manufacturing and design, with various hierarchically interwoven surfaces

Figure 6: Figure 10

Source: ChinaXiv —Machine translation. Verify with original.

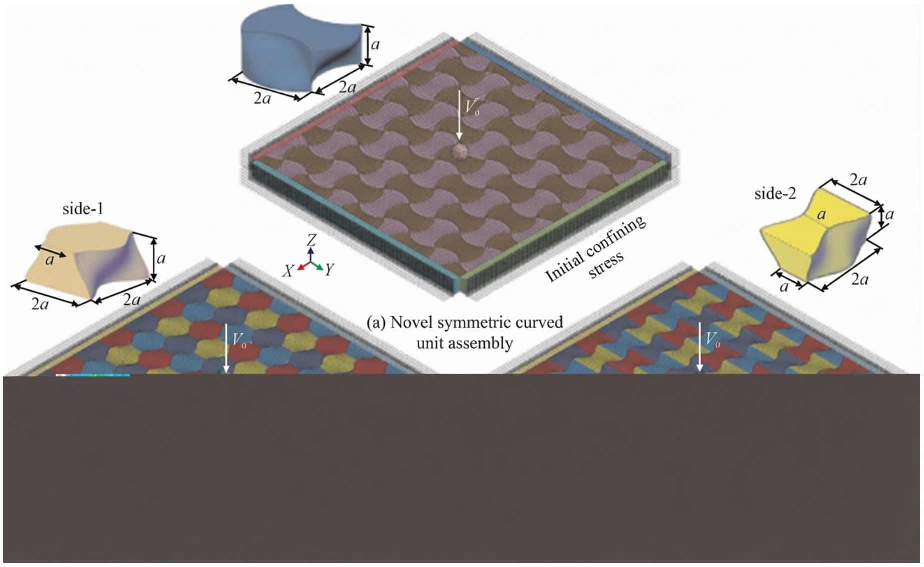

Figure 7: Figure 12

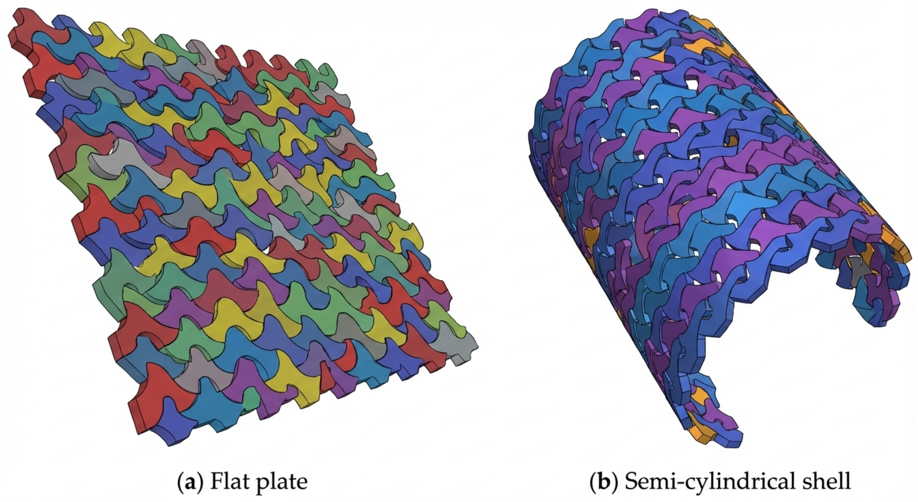
(a) Flat plate

(b) Semi-cylindrical shell

Figure 8: Figure 13